Cell, Vol. 114, 573–583, September 5, 2003, Copyright ©2003 by Cell Press

Visualization of the Target-Membrane-Inserted Fusion Protein of Semliki Forest Virus by Combined Electron Microscopy and Crystallography

Don L. Gibbons,[1] Inge Erk,[2] Brigid Reilly,[1] Jorge Navaza,[2] Margaret Kielian,[1,3,*] Félix A. Rey,[2] and Jean Lepault[2,3,*]

[1]Department of Cell Biology
Albert Einstein College of Medicine
1300 Morris Park Avenue
Bronx, New York 10461

[2]Virologie Moléculaire & Structurale
UMR 2472/1157 CNRS-INRA
1 Avenue de la Terrasse
91198 Gif-sur-Yvette Cedex
France

Summary

Semliki Forest virus enters cells by receptor-mediated endocytosis. The acidic environment of the endosome triggers a membrane fusion reaction that is mediated by the E1 glycoprotein. During fusion, E1 rearranges from an E1/E2 heterodimer to a highly stable, membrane-inserted E1 homotrimer (E1HT). In this study, we analyzed E1HT by a combination of electron cryomicroscopy, electron crystallography of negatively stained 2D crystals, and fitting of the available X-ray structure of the monomeric E1 ectodomain into the resulting 3D reconstruction. The visualized E1HT reveals that the ectodomain has reoriented vertically and inserted the distal tip of domain II into the lipid bilayer. Our data allow the visualization of a viral fusion protein inserted in its target membrane and demonstrate that insertion is a cooperative process, resulting in rings composed of five to six homotrimers.

Introduction

Regulated membrane fusion is integral to a number of biological processes, including vesicle trafficking, fertilization, and infection of cells by enveloped viruses (Blumenthal et al., 2003; Hernandez et al., 1996; Jahn et al., 2003). Of these, virus-membrane fusion is the leading paradigm for understanding the molecular mechanism of fusion and the structure and function of fusogenic proteins. The alphavirus Semliki Forest virus (SFV) has been extensively used to study virus entry and fusion and was the first virus shown to infect cells via low pH-triggered membrane fusion in endosomes (Helenius et al., 1980). The SFV membrane contains two transmembrane glycoproteins: the receptor binding E2 protein and the membrane fusion protein E1 (Schlesinger and Schlesinger, 2001). During biosynthesis, E1 and E2 associate as heterodimers in the endoplasmic reticulum, traffic through the secretory pathway, and assemble as trimeric spikes that direct budding of T = 4 icosahedral virus particles at the plasma membrane. Upon exposure to a pH of ~6.2 or below, the heterodimer dissociates and E1 undergoes a series of conformational changes. These result in the insertion of E1 into target membranes and the formation of a very stable E1 homotrimer (HT) that is required for fusion (Kielian et al., 1996; Wahlberg et al., 1992). Fusion of SFV requires the presence of cholesterol and sphingolipid in the target membrane, and these lipids act to promote the low pH-triggered conformational changes in E1 (Kielian et al., 2000; Wilschut et al., 1995).

The full-length E1 protein is a type I transmembrane protein of 438 amino acids attached to the viral membrane by a stretch of ~24 hydrophobic residues at its C terminus. E1 mediates fusion by a low-pH triggered interaction with the target and virus membranes. E1*, a proteolytic fragment of E1, has been extensively characterized for its membrane interaction and conformational changes at low pH (Ahn et al., 2002; Gibbons and Kielian, 2002; Kielian and Helenius, 1985; Klimjack et al., 1994). This ectodomain lacks 47 amino acids at the C terminus, including the transmembrane (TM) and juxtamembrane "stem" regions. A similar E1 fragment, termed E1-ΔS, was isolated from a complex of the SFV membrane proteins after digestion with subtilisin (Wengler et al., 1999). E1-ΔS was crystallized and its 3D structure determined to 0.35 nm resolution (Lescar et al., 2001). The structure shows that the E1 ectodomain is an elongated, rod-shaped molecule with three domains. The fusion peptide (residues 83–100) is located at the most viral membrane-distal tip, and the C terminus of the crystallized fragment is at the opposite, membrane-proximal end. The E1 fusion peptide was originally identified by its conserved and hydrophobic nature (Garoff et al., 1980), and subsequent mutagenesis data showed that this region is critical for fusion (Kielian et al., 1996). The fold of E1 is markedly similar to that of the membrane fusion proteins of the flaviviruses (Rey et al., 1995; Modis et al., 2003). The alphavirus and flavivirus fusion proteins have therefore been shown to be homologous and are now grouped together as class II viral membrane fusion proteins (Lescar et al., 2001), setting them apart from the remaining viral fusion proteins for which structures have been determined (class I). While E1* does not carry out membrane fusion due to the absence of the TM anchor, it undergoes very similar low pH-triggered conformational changes as full-length E1, including exposure of acid-specific monoclonal antibody epitopes and formation of a highly stable E1*HT. The interaction of the E1 ectodomain with target membranes is biochemically indistinguishable from that of the full-length, requiring low pH, cholesterol, and sphingolipid, and resulting in a membrane-inserted HT that can be isolated by cofloatation with target liposomes on sucrose density gradients (Klimjack et al., 1994).

The icosahedral symmetry of alphaviruses has enabled their study by electron cryomicroscopy and image processing. Reconstructions of SFV and the closely related Sindbis virus were fit with the crystal structure of the E1 ectodomain. This work revealed that in viral particles, E1 has its long axis oriented tangentially to the viral surface, forming an icosahedral shell around

*Correspondence: kielian@aecom.yu.edu (M.K.), mem-vms@gv.cnrs-gif.fr (J.L.)

the virus membrane (Lescar et al., 2001; Pletnev et al., 2001; Zhang et al., 2002). The E2 proteins lie on top of the E1 subunits, covering the fusion peptide and projecting away from the membrane surface to give the particle its "spiky" appearance. The observed E1/E2 dimer organization on the virus surface explains the importance of dimer dissociation in fusion. The overall arrangement suggests that the E1 proteins must undergo a conformational change and reorganization for the interaction of the fusion peptide with target membranes and the formation of E1HT.

The structural basis of class I viral fusion proteins has been extensively studied, following the seminal work on the influenza virus hemagglutinin (Skehel and Wiley, 2000). Class I proteins work by a common mechanism involving formation of a highly stable "hairpin" with a central α-helical coiled-coil (Eckert and Kim, 2001; Weissenhorn et al., 1999). Fusion is driven by the conversion of the metastable native trimer to the final stable hairpin with the fusion peptide and TM domains at the same end of a rod-shaped molecule (Melikyan et al., 2000), and is believed to be a cooperative process involving several trimers (Danieli et al., 1996; Markovic et al., 2001). The fusion peptide of class I proteins has been best characterized for influenza virus hemagglutinin (HA), where it has been positively identified by lipid photolabeling to lie within the amino terminal first 22 residues of the HA2 subunit (Harter et al., 1989). NMR studies of this peptide in a hydrophobic environment reveal an amphipathic structure that is predominantly helical with a central kink (Han et al., 2001). In contrast to class I, the class II fusion proteins contain primarily β sheet and convert from a native, less stable hetero- or homodimer to a highly stable trimer (Gibbons et al., 2000; Stiasny et al., 2001; Wahlberg et al., 1992). There are many important unknowns in the class II fusion mechanism, including the structural basis of membrane insertion and trimerization, the possibility of intertrimer cooperativity, and the role of specific lipids in these processes.

In this report, we present electron microscopic analyses of the full-length E1HT and the truncated E1*HT inserted in membranes. In both cases, the HTs were elongated structures with their long axes perpendicular to the membrane. Electron cryomicroscopy of the membrane bound HTs suggests that a substantial portion of E1 may insert into the target membrane. Insertion was observed as a cooperative process resulting in rings of five to six E1 trimers clustered together into patches at the liposome surface. In the case of E1*HT, this clustering resulted in an ordered hexagonal lattice containing exclusively rings of six trimers. Such 2D crystals were used to generate a 3D reconstruction of the negatively stained E1*HT to a resolution of $\sim$2.5nm. This reconstruction, which contains the extramembranous portion of the homotrimer, was fitted with the crystal structure of the native E1 ectodomain monomer. Our data suggest a model for the postfusion conformation of class II fusogenic proteins in which the E1*HT forms the central core of the molecule and the stem region and viral TM segment associate at its periphery, thus adopting a hairpin conformation similar to that observed for the class I fusion proteins.

Results

The Full-Length E1 Homotrimer

To maximize the efficiency of the conversion from virus-associated E1 to membrane-inserted HT, SFV particles were treated at low pH in the presence of an excess of target liposomes. Such treatment induces fusion, producing enlarged liposomes displaying E1HTs at their surface. These samples were then solubilized in n-octylglucoside (n-OG), and the E1HTs were purified by taking advantage of their resistance to proteases. Controlled proteolysis was thus used to digest the capsid, E2, and any nontrimerized E1. E1HTs were subsequently reconstituted into membranes and analyzed by electron microscopy. In general, the resulting samples were heterogeneous, displaying protein at the surface of liposomes of varying sizes and containing protein that appeared not to be clearly associated with membrane (Figure 1B). Thus, even under optimized conditions, the reconstitution is not efficient. Visualization of samples by negative staining (NS) showed that E1HTs are associated laterally in irregular clusters of rings containing five or six trimers (circled area in Figure 1A). These micrographs provided two characteristic views of the membrane-reconstituted E1HT. In top views, individual trimers were frequently found to display a donut-shaped appearance with outer and inner diameters of about 5 and 2 nm, respectively. Consistent with expectations from biochemical analysis, 3-fold rotational symmetry was observed when the molecules were appropriately oriented (inset, Figure 1A). The side views revealed an elongated domain projecting radially from the membrane, having a mean length and width of $\sim$7 and 5 nm, respectively. In general, the molecules are asymmetric, with a thin end pointing toward the liposome membrane. These images are similar to those observed by negative stain by Helenius in his pioneering work on reconstitution of deoxycholate-solubilized E1 (Helenius et al., 1977).

Electron cryomicroscopy (ECM) confirmed these observations of NS samples and revealed an additional structural feature of the E1HT (Figure 1B). As well as the density corresponding to the extramembrane domain, the side views reveal density within the lipid bilayer. Even in areas with relatively sparse protein, the zones of increased electron density within the membrane are contiguous with the projections of the extramembrane domain and, therefore, appear in register (arrows, Figure 1B). As expected from the presence of three TM domains per homotrimer, these data reveal that a substantial portion of the E1HT is inserted in the liposome membrane.

Both NS and ECM showed that the reconstituted E1HT was anchored into single liposomes rather than into two separate membranes by the two ends of the molecule. Because the samples were analyzed at high concentration, there are areas where liposomes overlap. However, there was no clear interaction of individual HTs with two membranes and, in fact, interaction between liposomes was often mediated by the protein contacts of the extramembrane domains interacting head-to-head (not shown). Overall, this suggests that in the final, postfusion conformation, both the TM domain and the fusion peptide segment of E1 lie at the thinner end of the cone-shaped molecule.

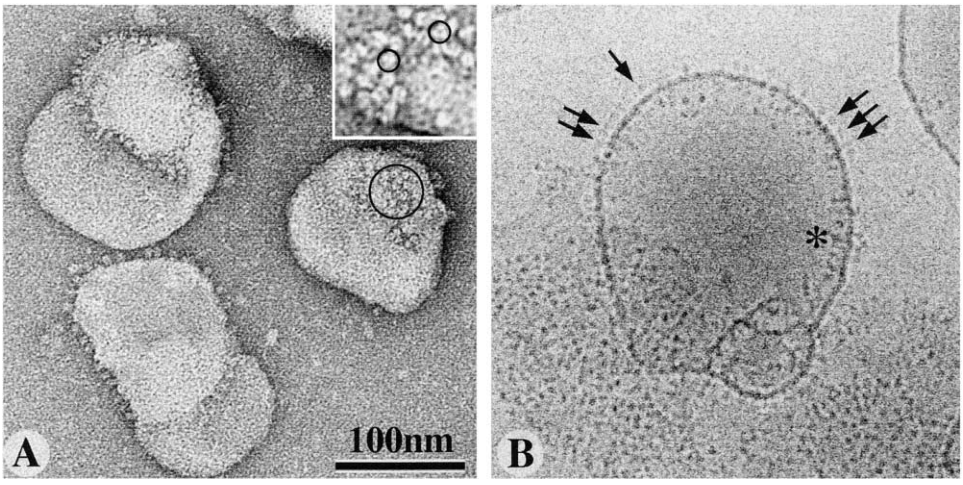

Figure 1. Purified Full-Length E1 Homotrimers Inserted in Liposomes

(A) Negatively stained (NS) samples. The E1HT appears as a cone-shaped object on the edge of the liposomes in side views. Donut-shaped objects are visualized in top views, forming irregular clusters of five or six trimers in the plane of the membrane (see circled area). Inset. The 3-fold symmetry can be visualized in appropriately oriented HT (circled) at 2× magnification.

(B) ECM of a vitrified E1HT-liposome sample. Side views show that each E1HT is associated with a membrane region of increased density (arrows). Protein projecting into the liposome is not easily distinguished from top views (asterisk).

It is difficult to tell from the images if the membrane reconstitution of E1HT occurs symmetrically or if the protein preferentially adopts a single right-side-out orientation. Side views of the extramembrane domain were easily recognized when it projected toward the outside of the liposome, but possible internal projections could easily be confused with top views (asterisk in Figure 1B). Since the incorporation of some E1HT molecules in the opposite orientation cannot be excluded, affecting the arrangement of the protein at the liposome surface, we studied liposomes into which the soluble E1 ectodomain (E1*) was inserted de novo by low pH treatment.

The E1* Homotrimer

Soluble E1* ectodomains insert into liposomes of the appropriate composition when the pH is lowered (Klimjack et al., 1994). Insertion is accompanied by a concomitant oligomerization of E1* into a stable homotrimer (E1*HT). NS electron micrographs of liposomes into which the E1*HT is inserted display protein clusters that are partially ordered (circled area, Figure 2A). This result is striking because the reaction was performed at a high lipid-to-protein ratio (LPR), suggesting that insertion is a cooperative process. Each individual E1*HT presents a roughly conical outline in side view (left inset, Figure 2A), with the thinner end facing the membrane. As a consequence, the intertrimer contacts appear to be localized to the membrane-distal end of the molecules. The elongated domain projects radially from the lipid bilayer, with a height of ~7 nm and a mean width of ~5 nm. Top views of E1*HT display a donut-shaped appearance, with outer and inner diameters equal to ~5 and 2 nm, respectively, and appear to display 3-fold rotational symmetry (right inset, Figure 2A). The dimensions and shape of E1*HT are thus similar to those of the full-length E1HT. Importantly, and in contrast to the E1HT, E1*HT associates within the plane of the membrane to form a regular hexagonal lattice containing interdigitating rings of six HT.

ECM showed that some liposomes contain small amounts of E1*HT generally found in clusters, while others were completely covered by an organized array of protein (Figure 2B). Top and side views of the protein on the liposomes appear as a regular hexagonal pattern and radially projecting spikes, respectively. These images are similar to those obtained by negative staining (Figure 2A), although less contrasted, as expected for unstained samples. Liposomes fully decorated with E1*HT (arrows, Figure 2B) displayed a rather uniform diameter and were smaller than those containing less protein. This suggests that E1*HT self-organizes upon interaction with liposomes and that insertion influences the liposome curvature and size. These properties were also observed with preparations of E1HT (data not shown). In agreement with these observations, liposomes presenting small patches of E1*HT generally displayed unusual morphologies in comparison to protein-free liposomes (inset, Figure 2B).

Similar to the results obtained with reconstituted E1HT, ECM of liposomes containing inserted E1*HT revealed that the extramembrane domains are associated with an in-register density variation within the membrane (arrowheads, Figure 2B; also Figure 3B, bottom). The periodic nature of the lateral protein interactions makes the density variation particularly clear. Such variations are not present in the protein-free liposomes (inset, Figure 2B). Thus, even in the absence of the E1 TM anchor, a protein density appears to be inserted into the lipid bilayer. We interpret this finding as arising from the existence of two functional domains of the E1*HT molecules: a membrane inserted (HT_M) and an extramembrane (HT_E) domain. However, due to the regular organization of the

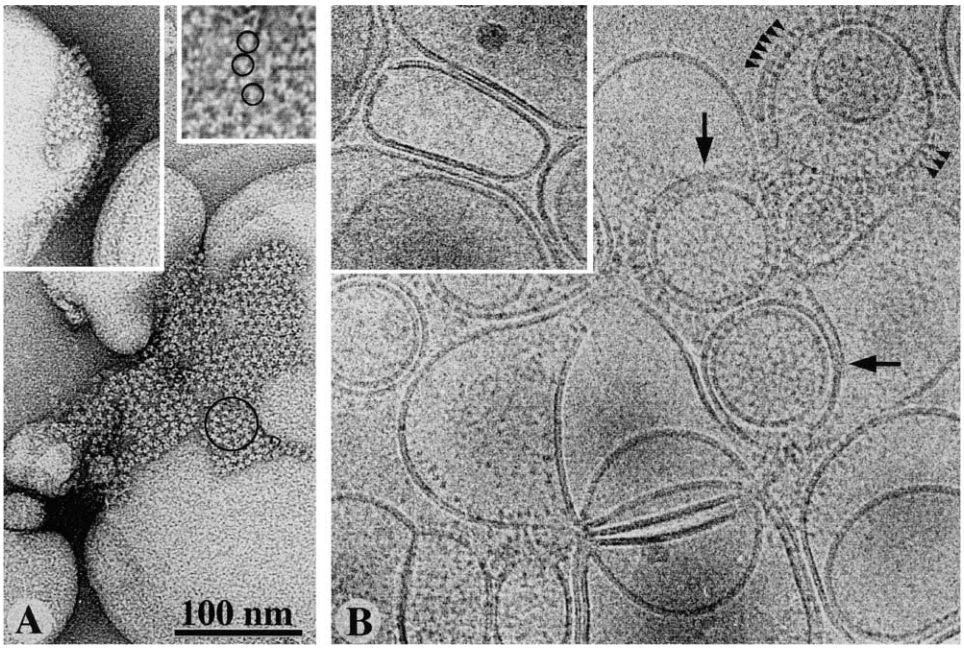

Figure 2. De Novo Insertion of the E1* Ectodomain Homotrimer into Membranes

(A) NS samples. Top views show the quasi-hexagonal lattice of E1*HT, and side views (inset, upper left) show the individual cone-shaped E1*HT projections. The 3-fold symmetry of molecules in the lattice can be distinguished at 2× magnification (inset, upper right).

(B) ECM. Liposomes show large variations in the amount of inserted E1*HT, and unusual morphologies are observed compared with pure liposomes (inset). The increased electron density within the lipid bilayer in contact with the E1*HT is indicated (arrowheads). Liposomes with a regular organization of E1*HT on the surface exhibit a rather constant diameter (arrows).

protein on the curved liposome surface and to the fact that micrographs represent a view of the sample in projection, we cannot exclude the possibility that superposition of two different molecules might partially explain the apparent intramembrane density. As a consequence, the depth of insertion of the protein into the membrane cannot be precisely determined.

To improve the quality of the 2D arrays of E1*HT produced upon de novo insertion into membranes and extend them into 2D crystals, the parameters governing their formation were investigated. Samples of membrane-inserted E1*HT were solubilized with n-OG, which completely dissociated the hexagonal lattice, but not the individual HT molecules, as visualized by negative staining (Figure 3A, central plate). Reconstitution after removal of varying amounts of lipid showed that the LPR was the most important factor controlling the lateral E1*HT interactions (Figure 3A). Reconstitution of the solubilized E1*HT-lipid mixture (at the original LPR) into liposomes revealed that the organization, orientation to the membrane, and dimensions of the protein were indistinguishable from those of E1*HT inserted de novo (Figure 3A, bottom left plate). However, at low LPR, rosettes of protein are observed (Figure 3A, top left). 2D planar crystals are observed when the LPR is increased, consistent with the formation of planar membrane patches (Figure 3A, top right). The more the LPR is increased, the more liposomes are observed, and the smaller the 2-D crystals are (Figure 3A, bottom right).

All of the E1*HT assemblies observed by NS were also found by ECM of the reconstituted samples. In particular, small 2D crystals were observed with the same properties as those visualized by NS (Figure 3B, top), demonstrating that the crystals are formed in solution during dialysis and not during the NS preparation. Because the contrast of such small objects is low, the crystals were difficult to localize in the ice film. Liposomes fully decorated by E1* and of rather uniform size were often observed (Figure 3B, bottom). In such samples, the reconstituted protein displayed features visually indistinguishable from those of the E1*HT inserted de novo into liposomes, with an extramembrane domain in register with an intramembrane density.

3D Reconstruction

In view of the difficulties encountered in the study of small 2D crystals in ice, electron crystallography studies were performed with NS E1*HT crystals (e.g., Figure 3A, upper right). The 2D crystals belong to the two-sided plane group p6 with cell parameter $a = 9.8$ nm. Even in NS samples, only small numbers of 2D crystals of the quality of the one boxed in Figure 3A were observed. Additionally, the quality of the crystals needed to be checked at high magnification, preventing the use of low-dose imaging conditions and resulting in greater beam damage. These factors limited the total number of views used for the 3D reconstruction and the resolution of the final structure. Although the crystals utilized were small, the coefficients of the Fourier transforms of their images displayed a significant signal-to-noise ratio up to a resolution of about 2 nm. The mean phase error between symmetry-related Fourier coefficients was less

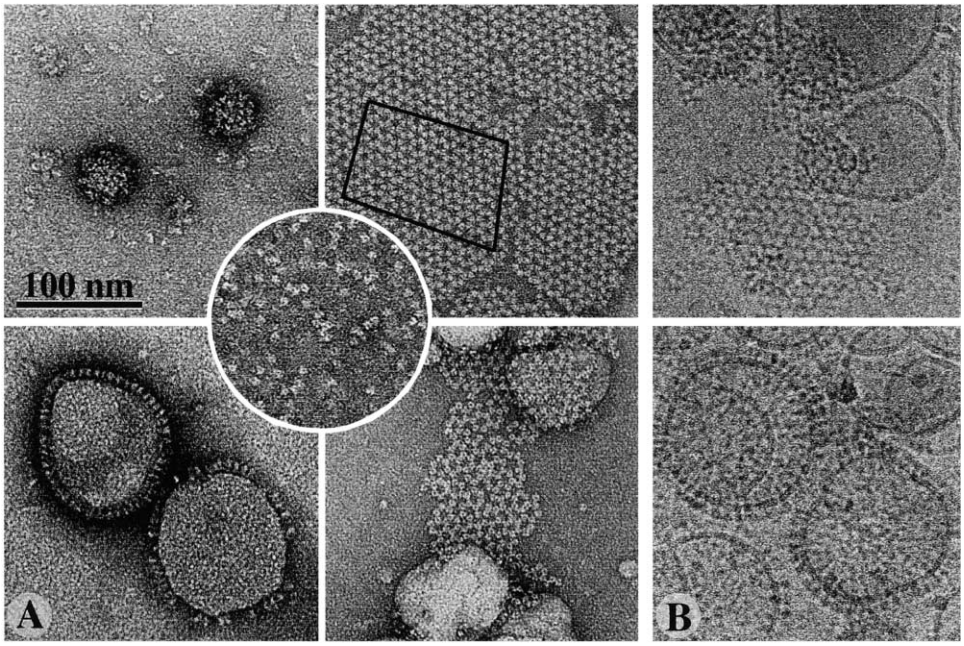

Figure 3. E1* Homotrimer Reconstituted at Varying LPR

(A) NS samples. E1*HT solubilized in n-OG showed the characteristic morphology of individual HTs (central plate). At low LPR, rosettes are visible after detergent dialysis (upper left). At higher lipid content, small 2D arrays are formed (upper right). The boxed area illustrates a typical crystal used to calculate the E1*HT 3D reconstruction. At increasing LPR, more liposomes are visible and the 2D HT arrays are smaller (lower right). Side views of the E1*HT inserted in liposomes are easily detected (lower left).

(B) ECM. 2D arrays (upper plate) and fully decorated liposomes (lower plate) are present in the vitrified samples. Clear periodic density variations are observed within the liposome membrane in register with the E1*HT projections.

than 15° at 2.5 nm resolution. The final reconstruction of the E1*HT was calculated with six images of untilted crystals and 28 images of crystals tilted up to 52°. The missing cone limits the resolution of the reconstruction along the z axis. The average phase error of individual measurements along the lattice within 0.08 nm windows along z* was less than 25°.

Figure 4 shows the 3D reconstruction of the E1* homotrimer, highlighting the two surfaces of the crystal and the interactions between six HT within the ring of the crystalline hexagonal lattice. In the left panel, the reconstruction is oriented to show a view of the thinner, target membrane-facing end of the HT, while in the right panel, it is oriented to show its thicker, outward-facing end. Each HT is a roughly cone-shaped object with a height and a mean diameter of ~7 and 5 nm, respectively, representing the extramembranous domain of the HT. The 3-fold rotational symmetry is best seen on the thick

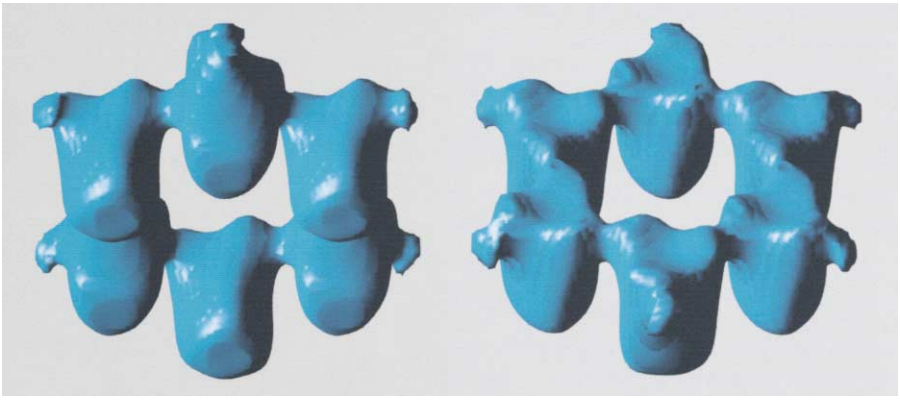

Figure 4. 3D Reconstruction of the E1*HT

A ring of six HTs is shown, as they are arranged in the 2D crystals. Left is a view of the target membrane-facing end of the E1*HT, and right shows a view of the thicker, membrane-distal end. Each E1*HT displays a roughly conical envelope.

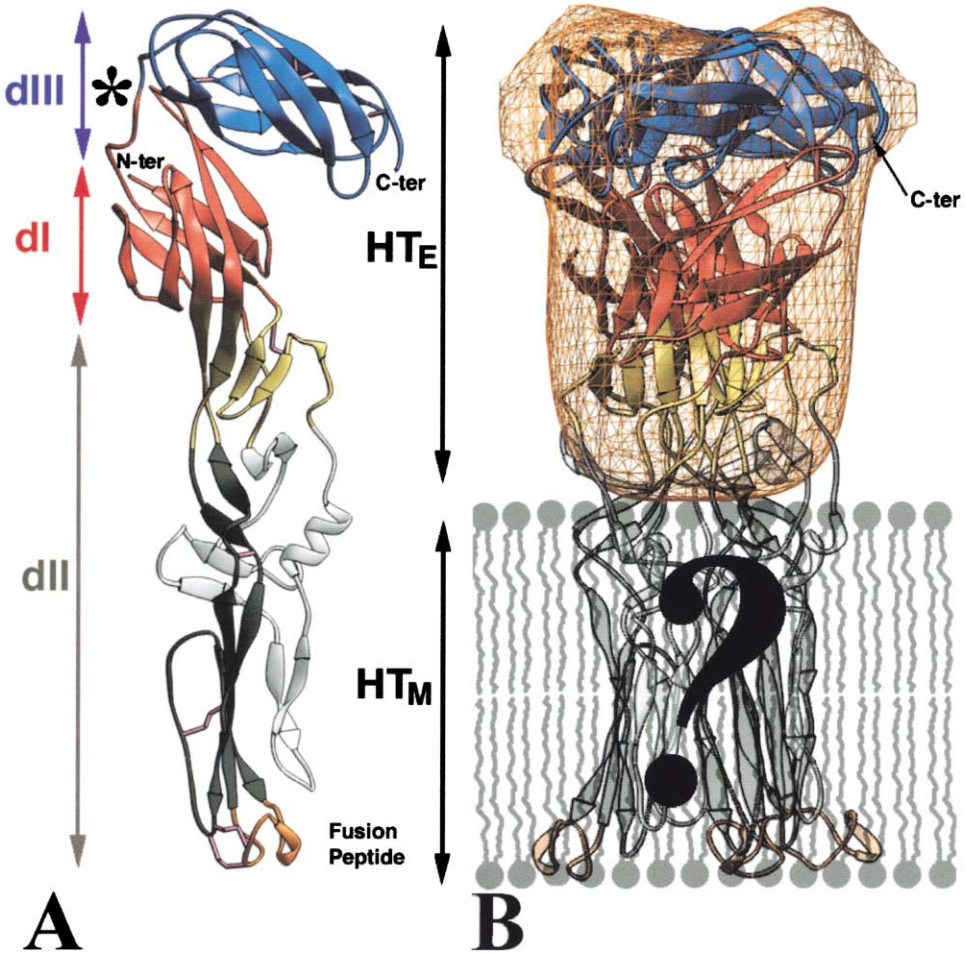

Figure 5. Fit of the Native E1* Atomic Model into the Reconstruction

(A) Ribbon representation of the E1* monomer structure as determined by X-ray crystallography (Lescar et al., 2001). E1* is composed of three domains: dI (red), dII (yellow and gray), and dIII (blue), and has an overall length of ~12nm. One end of the molecule was assigned as the extramembrane domain (HT_E, ~7nm in length) and the other the membrane-inserted domain (HT_M, ~5 nm). The flexible connection between dI and dIII is indicated by the asterisk.

(B) Pseudoatomic model for the E1*HT derived by fitting the E1* fragment into the EM reconstruction as a trimer with an automated procedure (Navaza et al., 2002). The 3D reconstruction is represented as a gold-colored mesh frame. The best solution for fitting an atomic model into the EM reconstruction is achieved when the blue, red, and yellow regions are used, leaving out the membrane-inserted domain indicated in gray. The C terminus of the E1 fragment, connecting to the stem/anchor region, is indicated. The membrane is represented by the gray lipids. In the model, all gray segments of the protein are hypothetical as the region may change its fold with respect to the monomer (thus the question mark) and are shown only to give a rough idea of its relative proportion and location with respect to the observed region (in colors), as extrapolated from the ECM and NS observations.

end of the molecule (right panel). The internal diameter of the ring defined by six E1*HT is ~7 nm. The interactions between the E1*HTs in the ring take place at the membrane-distal end. The features of the reconstruction agree with the visual observations of the E1*HT on membranes both by NS and ECM, allowing an unambiguous orientation of the molecules. To better interpret this structure, the available atomic model of the E1 ectodomain, derived previously by X-ray crystallography (Lescar et al., 2001), was fitted into the EM reconstruction.

Fitting of the Atomic Model of E1* into the 3D Reconstruction

The crystallized ectodomain is a 12 nm long rod-shaped molecule with the fusion peptide on one end (Figure 5A). The molecule has three domains and appears to have a flexible connection between domains I and III (indicated by an asterisk). Assuming there are no conformational changes between the domains of the protein and that the membrane-inserted region completely traverses the lipid bilayer, the long dimension of the ectodomain fits the total length of the E1*HT (~7 nm for the extramembrane domain plus ~5 nm for the membrane-inserted domain). With these assumptions in mind and in order to fit the monomer into our 3D reconstruction, intra- and extramembrane domains were defined within the atomic model. The most plausible orientation of the rod-like molecule would have the fusion-peptide-containing domain II inserted in the lipid bilayer. The putative membrane-inserted region HT_M (with the fusion peptide at its far end) was therefore cut at 5 nm from the fusion

Table 1. Statistics of the Rigid-Body Fitting into the EM Reconstruction

	Correlation Coefficient (CC)[A]	R Factor[a]	Clash Factor[b]	Temperature Factor B[c] (nm^2)
E1-dIII + dI + dII[d]	0.95	0.31	0.11	17.50
E1-dII	0.90	0.38	0.20	24.16
CD4, domains 1 + 2[e]	0.90	0.37	0.28	25.75

[a] $CC = \Sigma_h (F_{obs}{}^h F_{calc}{}^{*h})/\{\Sigma_h (A_{obs}{}^h)^2 (A_{calc}{}^h)^2\}^{1/2}$ and R factor $= \Sigma_h (A_{obs}{}^h - A_{calc}{}^h)/ \Sigma_h A_{obs}{}^h$, where F_{obs} and F_{calc} are the complex Fourier coefficient and $A_{obs}$and A_{calc} are the amplitudes of the observed and calculated Fourier coefficient, respectively. The asterisk denotes complex conjugation. "Observed" means calculated from the experimental map, and "calculated" are calculated from the atomic model using X-ray atomic scattering factors.

[b] Clash factor defined as the ratio between the number of residues in overlapping areas over the total number of residues.

[c] B is defined such as as $(A_{obs})^2 = (A_{calc})^2 \exp(-Bs^2/4)$, where s is the amplitude of the scattering vector.

[d] This fragment contained the blue, red, and yellow parts of E1* (HT_E), as indicated in Figure 5.

[e] CD4 coordinates were taken from the PDB, accession code number 1G9M.

peptide and is indicated in gray, with the fusion peptide in orange in Figure 5A. The remaining polypeptide, termed HT_E, (in red, blue, and yellow) was used to fit the extramembrane domain as a single rigid entity. The HT_E fragment can readily be fitted as a trimer into the reconstruction by a least-squares minimization procedure with the automated program URO (Navaza et al., 2002). This program maximizes the overlap between the atomic model and the density of the EM reconstruction without considering possible clashes between subunits. Therefore, an important measure of the quality of the fit is the number of resulting clashes. In the current fit, the clashes (about 10% of the residues) are restricted to domain I, suggesting a possible rearrangement of this domain with respect to domain III. Although there is room in the volume of the reconstruction to reorient domain I to avoid these clashes, we have not attempted more than a single-body fit given the limited resolution. The possibility of an altered orientation between these two domains due to the fusogenic conformational change is considered further in the Discussion section. To assess the meaningfulness of the solution, we fitted as controls the molecule cut in the opposite way (a 7 nm fragment starting from the tip of domain II) or an unrelated rod-shaped molecule (CD4 domains 1 and 2). In both cases, poorer solutions were found as indicated by the lower correlation coefficient, higher R factor, or important clashes between subunits. Table 1 shows the corresponding statistics obtained from the fit of HT_E and the controls.

The resulting fit of HT_E into the reconstruction gave rise to a slightly twisted structure with domain III at the top (most membrane distal), domain I in the middle, and part of domain II at the membrane proximal end (Figure 5B). Domain III dominated the fit by occupying the thicker region of the reconstruction at the top of the EM density with the C terminus pointing toward the external surface of the resulting pseudoatomic HT model. Domain I fits underneath, but there are no specific features at this resolution in the 3D reconstruction that can guide a clear orientation of this domain.

Discussion

ECM allows imaging of unstained biological samples owing to the actual electron density variations between a protein and its natural environment. This allowed us to observe simultaneously the density difference between the E1 extramembrane domain and the aqueous solvent, and between its membrane domain and the lipid bilayer, thus achieving the visualization of a fusion protein in a postfusion conformation inserted in its target membrane. Visualization was aided by the regular organization of E1*HT on liposomes, giving rise to periodic density variations within the membrane, in register with the density outside. Although we cannot be certain about the depth of membrane insertion of the protein, these images extend the conclusion of prior biochemical studies that the "fusion peptide" loop of E1 inserts into the target membrane by indicating that an additional portion of the protein may also insert. Available data (Ahn et al., 2002; Kielian et al., 1996) demonstrate that the fusion peptide is essential to the membrane insertion of E1 and the fusion event. In fact, a monoclonal antibody targeting the fusion peptide blocks membrane insertion of E1* (D.L.G. and M.K., unpublished data). The observations are also compatible with experiments involving treatment of the membrane-inserted E1*HT with reducing agents, which destabilize the disulfide-crosslinked domain II. Under these conditions, limited proteolysis of the E1*HT releases a soluble form lacking a portion of domain II including the fusion peptide (Gibbons and Kielian, 2002).

The HTs in the postfusion state are oriented perpendicular to the membrane and make intertrimer contacts at the membrane-distal end of the molecules, demonstrating extensive rearrangement from their original position on the virus membrane (Lescar et al., 2001). The finding that the E1*HTs inserted in the membrane are present in rings that cluster into patches strongly suggests cooperativity in the membrane-insertion process. Interestingly, the formation of ring-like assemblies of fusion proteins has been previously observed in studies of rabies and influenza virus (Gaudin et al., 1996; Kanaseki et al., 1997), and cooperativity has been proposed to be an important factor in the membrane fusion activity of many different viruses (Blumenthal et al., 1996; Danieli et al., 1996; Markovic et al., 2001; Plonsky and Zimmerberg, 1996; Roche and Gaudin, 2002). The observed rings of HTs could allow the proteins to act in concert in the formation of the initial fusion pore. Liposomes completely covered with E1HT or E1*HT exhibit rather uniform sizes, suggesting that the interactions of the protein "coat" also influence membrane curvature. The cooperative interactions may therefore contribute to

membrane fusion by potentiating the protein conformational changes, membrane insertion, and subsequent effects on membrane curvature.

The 3D reconstruction was calculated from NS 2D crystals associated with flat membranes and therefore only contains the extramembrane portion of the HT because the hydrophilic staining compounds do not penetrate membranes. It is reasonable to assume that domains I and III of the atomic model, which lie at the end of the molecule opposite from the fusion peptide (see Figure 5A), constitute the extramembrane region of E1HT. Indirect evidence suggests that domains I and III are each likely to maintain the same fold in all conditions. First, domains I and III are both very well structured β-barrels, i.e., displaying a highly stable fold, and it is therefore difficult to envision a major refolding within these domains during membrane fusion. Second, for the homologous glycoprotein E from TBE virus, the conformational epitopes in domain III are preserved after the acid-induced conformational change, while those in domain II are lost (Rey et al., 1995). The pseudoatomic model of the E1*HT (Figure 5B) thus provides a plausible organization of domains I and III within the trimer, with the C terminus of domain III pointing laterally toward the outside of the molecule. In such a model, trimerization involves extensive contacts along the length of the subunit molecules, in keeping with the significant biochemical stability of the E1HT (Gibbons and Kielian, 2002; Wahlberg et al., 1992).

Several assumptions were made in the generation of the pseudoatomic model presented in Figure 5B, guided by the observations presented in Figures 1–3. (1) The length of the E1* subunit is unaffected by the conformational change, and (2) the inserted portion may span the lipid bilayer. However, as indicated in Figure 5A, there is a flexible connection between domains I and III. If movement occurs at this connection to bring the body of domain III back against domains I and II, the total length of the molecule would be less than 12 nm. Since the observed projecting domain seen in images and the reconstruction is ~7 nm, the subsequent depth of membrane insertion would therefore be less than suggested in Figure 5B. To illustrate this uncertainty in the conformational changes not discernable at the resolution of the reconstruction, Figure 6A presents a sketch of the two extreme alternative models for the E1*HT inserted into a membrane (M).

In the first model for membrane insertion of the HT, the fusion peptide of domain II lies at the internal side of the membrane and would be deeply anchored into the bilayer (Figure 5B and 6A, left). Insertion to form a membrane-spanning structure would require significant refolding of domain II in order to avoid exposing main chain polar groups to the aliphatic environment of the membrane. The model on the right has the protein inserted to a lesser degree, and it is not necessary to postulate such a substantial structural change of this domain to mediate membrane interaction. From biochemical experiments it is clear that insertion of E1* into the target membrane requires the presence of cholesterol and sphingolipids (Ahn et al., 2002; Klimjack et al., 1994), which are also required for alphavirus-triggered membrane fusion (Kielian et al., 2000; Wilschut et al., 1995). The lipid dependence of fusion can be modulated

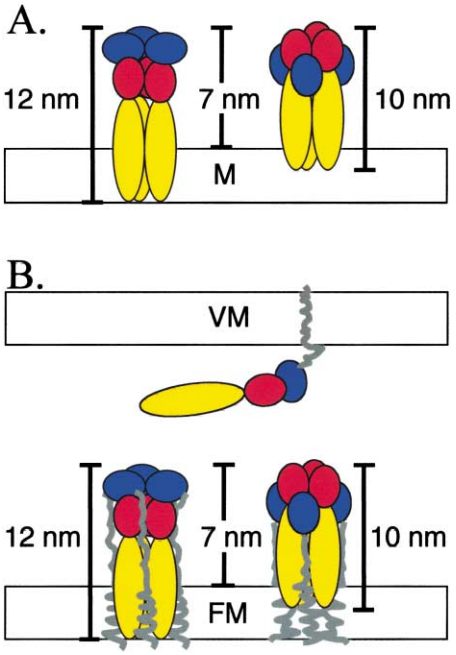

Figure 6. Model for the Conformational Changes and Membrane Insertion of E1

(A) The proposed model of the E1*HT after insertion into a membrane (M) as a vertical trimer. The three domains of E1* are colored as in Figure 5. The fusion peptide is located at the very tip of the yellow domain II. On the left is the E1*HT subunit without significant conformational change, spanning the membrane (as in Figure 5B). On the right, movements have been introduced around the flexible domain I/III connection to reflect the possibility that the HT inserts less deeply into the membrane.

(B) The top illustrates the native conformation of E1 on the viral membrane (VM). It is held in this tangential orientation through interactions with E2 (not shown) and lateral contacts in the T = 4 icosahedral particle (Lescar et al., 2001; Zhang et al., 2002). The stem/transmembrane region is shown in gray. At the bottom, similar conformations as in (A) are shown for the E1HT, with the stem/anchor region drawn in to show how E1*HT and E1HT can appear similar in the EM images. As for class I fusion proteins, in the model the C-terminal stem/anchor regions would associate at the periphery of the trimer, with the viral TM region next to the fusion peptide in the fused membrane (FM).

by single amino acid changes in E1, such as srf-3, -4 and -5, point mutations that decrease the cholesterol and/or sphingolipid requirements (Chatterjee et al., 2002; Vashishtha et al., 1998). Interestingly, all three mutations map to domain II, supporting the idea that insertion of a portion of domain II is facilitated by specific lipid interactions. Unfortunately, along with the uncertainty on the degree of membrane insertion, our low-resolution data provide no information about the actual fold of this region, and it is therefore not possible to discriminate between the two models presented in Figure 6A. Only studies at much higher resolution, either by using electron diffraction with better quality 2D crystals or X-ray diffraction of single 3D crystals, can provide such an answer.

Comparison of the images of the full-length E1HT and the truncated E1*HT on membranes showed that the two

exhibit very similar shapes and dimensions, strongly indicating that in the final postfusion conformation the TM anchor is on the same side of the molecule as the membrane-inserted domain II. Figure 6B illustrates the starting conformation of the E1 protein as it lies on the viral membrane (VM) and indicates how after the conformational change the stem region could traverse the exterior surface of the trimer down through the fused membrane (FM). Two extreme final conformations for the full-length E1HT are presented as for the E1*HT to account for possible rearrangements in the protein and different depths of protein insertion. These models suggest that, as for class I fusion proteins, transition to the postfusion conformation may bring the virus and target membranes together via a strong interaction of the stem region with the periphery of the extramembranous part of the HT. The E1*HT would thus be analogous to the central coiled-coil of class I fusion proteins, and the E1 "stem" would resemble their external C-terminal segment, resulting in an overall similar hairpin conformation. The general mechanism of membrane fusion by class I and class II fusion proteins may therefore be very similar, despite the completely different structural organization of the fusogenic proteins.

Experimental Procedures

Virus Purification

SFV was propagated in BHK-21 cells and purified by banding on tartrate gradients as previously described (Kääriäinen et al., 1969).

Liposomes

Liposomes were prepared by freeze-thaw and extrusion as previously described (Chatterjee et al., 2002) using a molar ratio of 1:1:1:3 phosphatidylcholine:phosphatidylethanolamine:sphingomyelin (bovine brain):cholesterol. Liposome stocks contained ^{3}H-cholesterol as a tracer for lipid quantitation.

Preparation of Full-Length E1 Homotrimer (E1HT)

Purified virus (0.5 mg/ml) was mixed with liposomes (1 mM), treated at pH 5.5 for 10 min at 20°C, and adjusted to neutral pH. The samples were solubilized in 1% n-OG for 1 hr at room temperature, followed by a brief digestion with RNase A and trypsin (50 μg/ml). The digestion was stopped by addition of PMSF, and the trimers were isolated in a microconcentrator. SDS-PAGE analysis demonstrated that >90% of the protein preparation was full-length trimeric E1.

Preparation of SFV Glycoprotein Ectodomains

Soluble forms of the E1 and E2 spike protein subunits (E1* and E2*) were prepared as previously described (Gibbons and Kielian, 2002; Kielian and Helenius, 1985).

Formation and Sucrose Density Gradient Flotation of the Liposome-Inserted E1* Homotrimer

Purified ectodomains (0.25 mg/ml) were mixed with liposomes (1 mM), treated at pH 5.5 for 10 min at 37°C, and then adjusted to neutral pH. The liposome-inserted ectodomain homotrimer (E1*HT) was separated from the E2* and monomeric E1* by cofloatation of the HT with liposomes on sucrose step gradients, all as previously described (Ahn et al., 2002). The initial LPR of the E1* HT preparation was approximately one HT per 2600 lipid molecules.

Two-Dimensional Crystallization

The E1HT did not crystallize under any of the conditions investigated. The LPR was found to control the crystallization of E1*HT. An adapted version of the in situ crystallization method was utilized (Yeager et al., 1999). Instead of reconstitution of fully purified protein into lipid membranes, the protocol concentrates the protein previously inserted into membranes by treatment with a dialyzable detergent to partially remove the lipids. In brief, liposome-inserted E1*HT taken from the top of sucrose floatation gradients was solubilized in n-OG, and lipids were gradually removed by differential filtration on 100 kDa cutoff microconcentrators. Small volumes (50–250 μl) of the resulting samples were then dialyzed against 500 ml of detergent-free buffer for 18–24 hr at room temperature or 4°C. The LPR was estimated from the protein concentration and the amount of residual radioactive lipids. The optimal conditions for solubilization were 0.7%–1% octylglucoside, supplemented with 20 mM octyl-thioglucoside. The best crystals were obtained when the samples were dialyzed against 150 mM NaCl and 50 mM Tris-HCl (pH 8.35) at room temperature.

Electron Microscopy

Samples were stained with solutions of 2% uranyl acetate (UA) or sodium phospho-tungstic acid (pH 7.0 or 8.0). No appreciable difference was observed between the two stains, and UA was used for most of the samples presented, including the images for the reconstruction. ECM was performed as previously described (Lepault et al., 1983) on a Philips CM12 electron microscope operated at 100 kV. Images were recorded at a magnification of 35000×.

Image Processing and 3D Reconstruction

The quality of the negatives was controlled on an optical bench. Images were selected on the quality of their optical diffraction pattern: no astigmatism, under focus of ~1 μm, significant Fourier coefficients at 0.33 nm^{-1}. Retained images were digitized with an Optronics P1000 scanner using a 25 μm raster size and processed with the programs written at the MRC-LMB (Crowther et al., 1996). Briefly, images were corrected for lattice deformations (Henderson et al., 1986). Calculation of the Fourier transforms, indexing of the reciprocal lattice, extraction, and interpolation of the Fourier coefficients were performed as described (Amos et al., 1982). Scaling of amplitudes and refinement of phases to a common origin was carried out between reflections within 0.066 nm^{-1}. Preliminary analysis was done in p1, and since the phase behavior corresponded closely to that of p6, the refinement was carried out in this space group. The combined data for the final reconstruction presented in Figure 4 included ten-layer lines to a maximum resolution of 2 nm in the (x,y)* plane and 2.5nm in z*. These curves were then fitted with a sinc function and interpolated at intervals of 0.066 nm^{-1}. Fourier syntheses were calculated with 180 coefficients in the asymmetric unit. Figure 4 was generated by contouring the density of the reconstruction to 0.75 σ, a level at which there is no disconnected mass, and without the application of an isotropic resolution filter. This level of contour accounts for ~75% of the expected mass of the molecule.

Fitting of the Crystallographic E1* Monomer into the Reconstruction

Portions of the atomic model for the E1 monomer (PDB accession number 1I9W; missing loops in this structure were modeled for illustration purposes) were used as outlined in the text for a rigid-body fit into the EM reconstruction (Navaza et al., 2002). The fitting was done with the molecule cut as indicated in the text and in Figure 5.

Acknowledgments

We thank Y. Gaudin for comments on the manuscript and S. Bressanelli, S. Duquerroy, J. Lescar, A. Roussel, M.C. Vaney, and the members of our laboratories for help and discussions. We acknowledge support from the CNRS and INRA, the SESAME Program of the Région Ile-de-France, the French Fondation pour la Recherche Médicale, the Association pour la Recherche contre le Cancer, and the CNRS programs Physique et Chimie du Vivant and Dynamique et réactivité des assemblages biologiques. The work was also supported by a grant to M.K. from the Public Health Service (R01 GM52929) and by Cancer Center Core Support Grant NIH/NCI P30-CA13330. D.L.G. was supported through the Medical Scientist Training Program of the Albert Einstein College of Medicine (NIH T32 GM 07288) and the Albert Cass Traveling Fellowship. Data in this paper are from a thesis submitted by D.L.G. in partial fulfillment of the requirements for the Degree of Doctor of Philosophy in the Sue

Golding Graduate Division of Medical Sciences, Albert Einstein College of Medicine, Yeshiva University.

Received: April 14, 2003
Revised: August 4, 2003
Accepted: August 12, 2003
Published: September 4, 2003

References

Ahn, A., Gibbons, D.L., and Kielian, M. (2002). The fusion peptide of Semliki Forest virus associates with sterol-rich membrane domains. J. Virol. *76*, 3267–3275.

Amos, L., Henderson, R., and Unwin, P. (1982). Three-dimensional structure determination by electron microscopy of two-dimensional crystals. Prog. Biophys. Mol. Biol. *39*, 183–231.

Blumenthal, R., Sarkar, D.P., Durell, S., Howard, D.E., and Morris, S.J. (1996). Dilation of the influenza hemagglutinin fusion pore revealed by the kinetics of individual cell-cell fusion events. J. Cell Biol. *135*, 63–71.

Blumenthal, R., Clague, M.J., Durell, S.R., and Epand, R.M. (2003). Membrane fusion. Chem. Rev. *103*, 53–69.

Chatterjee, P.K., Eng, C.H., and Kielian, M. (2002). Novel mutations that control the sphingolipid and cholesterol dependence of the Semliki Forest virus fusion protein. J. Virol. *76*, 12712–12722.

Crowther, R.A., Henderson, R., and Smith, J.M. (1996). MRC image processing programs. J. Struct. Biol. *116*, 9–16.

Danieli, T., Pelletier, S.L., Henis, Y.I., and White, J.M. (1996). Membrane fusion mediated by the influenza virus hemagglutinin requires the concerted action of at least three hemagglutinin trimers. J. Cell Biol. *133*, 559–569.

Eckert, D.M., and Kim, P.S. (2001). Mechanisms of viral membrane fusion and its inhibition. Annu. Rev. Biochem. *70*, 777–810.

Garoff, H., Frischauf, A.-M., Simons, K., Lehrach, H., and Delius, H. (1980). Nucleotide sequence of cDNA coding for Semliki Forest virus membrane glycoproteins. Nature *288*, 236–241.

Gaudin, Y., Raux, H., Flamand, A., and Ruigrok, R.W.H. (1996). Identification of amino acids controlling the low-pH-induced conformational change of rabies virus glycoprotein. J. Virol. *70*, 7371–7378.

Gibbons, D.L., and Kielian, M. (2002). Molecular dissection of the Semliki Forest virus homotrimer reveals two functionally distinct regions of the fusion protein. J. Virol. *76*, 1194–1205.

Gibbons, D.L., Ahn, A., Chatterjee, P.K., and Kielian, M. (2000). Formation and characterization of the trimeric form of the fusion protein of Semliki Forest virus. J. Virol. *74*, 7772–7780.

Han, X., Bushweller, J.H., Cafiso, D.S., and Tamm, L.K. (2001). Membrane structure and fusion-triggering conformational change of the fusion domain from influenza hemagglutinin. Nat. Struct. Biol. *8*, 715–720.

Harter, C., James, P., Bachi, T., Semenza, G., and Brunner, J. (1989). Hydrophobic binding of the ectodomain of influenza hemagglutinin to membranes occurs through the fusion peptide. J. Biol. Chem. *264*, 6459–6464.

Helenius, A., Fries, E., and Kartenbeck, J. (1977). Reconstitution of Semliki Forest virus membrane. J. Cell Biol. *75*, 866–880.

Helenius, A., Kartenbeck, J., Simons, K., and Fries, E. (1980). On the entry of Semliki Forest virus into BHK-21 cells. J. Cell Biol. *84*, 404–420.

Henderson, R., Baldwin, J., Downing, K., Lepault, J., and Zemlin, F. (1986). Structure of purple membrane from Halobacterium halobium: recording, measurement and evaluation of electron micrographs at 3.5Å resolution. Ultramicroscopy *19*, 147–178.

Hernandez, L.D., Hoffman, L.R., Wolfsberg, T.G., and White, J.M. (1996). Virus-cell and cell-cell fusion. Annu. Rev. Cell Dev. Biol. *12*, 627–661.

Jahn, R., Lang, T., and Sudhof, T.C. (2003). Membrane fusion. Cell *112*, 519–533.

Kääriäinen, L., Simons, K., and von Bonsdorff, C.-H. (1969). Studies of Semliki Forest virus subviral components. Ann. Med. Exp. Biol. Fenn. *47*, 235–248.

Kanaseki, T., Kawasaki, K., Murata, M., Ikeuchi, Y., and Ohnishi, S. (1997). Structural features of membrane fusion between influenza virus and liposome as revealed by quick-freezing electron microscopy. J. Cell Biol. *137*, 1041–1056.

Kielian, M., and Helenius, A. (1985). pH-induced alterations in the fusogenic spike protein of Semliki Forest Virus. J. Cell Biol. *101*, 2284–2291.

Kielian, M., Klimjack, M.R., Ghosh, S., and Duffus, W.A. (1996). Mechanisms of mutations inhibiting fusion and infection by Semliki Forest virus. J. Cell Biol. *134*, 863–872.

Kielian, M., Chatterjee, P.K., Gibbons, D.L., and Lu, Y.E. (2000). Specific roles for lipids in virus fusion and exit: examples from the alphaviruses. In Subcellular Biochemistry Volume 34. Fusion of Biological Membranes and Related Problems, H. Hilderson and S. Fuller, eds. (New York: Plenum Publishers), pp. 409–455.

Klimjack, M.R., Jeffrey, S., and Kielian, M. (1994). Membrane and protein interactions of a soluble form of the Semliki Forest virus fusion protein. J. Virol. *68*, 6940–6946.

Lepault, J., Booy, F.P., and Dubochet, J. (1983). Electron microscopy of frozen biological suspensions. J. Microsc. *129*, 89–102.

Lescar, J., Roussel, A., Wien, M.W., Navaza, J., Fuller, S.D., Wengler, G., and Rey, F.A. (2001). The fusion glycoprotein shell of Semliki Forest virus: an icosahedral assembly primed for fusogenic activation at endosomal pH. Cell *105*, 137–148.

Markovic, I., Leikina, E., Zhukovsky, M., Zimmerberg, J., and Chernomordik, L.V. (2001). Synchronized activation and refolding of influenza hemagglutinin in multimeric fusion machines. J. Cell Biol. *155*, 833–844.

Melikyan, G.B., Markosyan, R.M., Hemmati, H., Delmedico, M.K., Lambert, D.M., and Cohen, F.S. (2000). Evidence that the transition of HIV-1 gp41 into a six-helix bundle, not the bundle configuration, induces membrane fusion. J. Cell Biol. *151*, 413–423.

Modis, Y., Ogata, S., Clements, D., and Harrison, S.C. (2003). A ligand-binding pocket in the dengue virus envelope glycoprotein. Proc. Natl. Acad. Sci. USA *100*, 6986–6991.

Navaza, J., Lepault, J., Rey, F.A., Alvarez-Rua, C., and Borge, J. (2002). On the fitting of model electron densities into EM reconstructions: a reciprocal-space formulation. Acta Crystallogr. D Biol. Crystallogr. *58*, 1820–1825.

Pletnev, S.V., Zhang, W., Mukhopadhyay, S., Fisher, B.R., Hernandez, R., Brown, D.T., Baker, T.S., Rossmann, M.G., and Kuhn, R.J. (2001). Locations of carbohydrate sites on alphavirus glycoproteins show that E1 forms an icosahedral scaffold. Cell *105*, 127–136.

Plonsky, I., and Zimmerberg, J. (1996). The initial fusion pore induced by baculovirus GP64 is large and forms quickly. J. Cell Biol. *135*, 1831–1839.

Rey, F.A., Heinz, F.X., Mandl, C., Kunz, C., and Harrison, S.C. (1995). The envelope glycoprotein from tick-borne encephalitis virus at 2A resolution. Nature *375*, 291–298.

Roche, S., and Gaudin, Y. (2002). Characterization of the equilibrium between the native and fusion-inactive conformation of rabies virus glycoprotein indicates that the fusion complex is made of several trimers. Virology *297*, 128–135.

Schlesinger, S., and Schlesinger, M.J. (2001). *Togaviridae*: the viruses and their replication. In Fields Virology, D.M. Knipe, and P.M. Howley, eds. (Philadelphia: Lippincott, Williams and Wilkins), pp. 895–916.

Skehel, J.J., and Wiley, D.C. (2000). Receptor binding and membrane fusion in virus entry: The influenza hemagglutinin. Annu. Rev. Biochem. *69*, 531–569.

Stiasny, K., Allison, S.L., Mandl, C.W., and Heinz, F.X. (2001). Role of metastability and acidic pH in membrane fusion by tick-borne encephalitis virus. J. Virol. *75*, 7392–7398.

Vashishtha, M., Phalen, T., Marquardt, M.T., Ryu, J.S., Ng, A.C., and Kielian, M. (1998). A single point mutation controls the cholesterol dependence of Semliki Forest virus entry and exit. J. Cell Biol. *140*, 91–99.

Wahlberg, J.M., Bron, R., Wilschut, J., and Garoff, H. (1992). Membrane fusion of Semliki Forest virus involves homotrimers of the fusion protein. J. Virol. *66*, 7309–7318.

Weissenhorn, W., Dessen, A., Calder, L.J., Harrison, S.C., Skehel, J.J., and Wiley, D.C. (1999). Structural basis for membrane fusion by enveloped viruses. Mol. Membr. Biol. *16*, 3–9.

Wengler, G., Wengler, G., and Rey, F.A. (1999). The isolation of the ectodomain of the alphavirus E1 protein as a soluble hemagglutinin and its crystallization. Virology *257*, 472–482.

Wilschut, J., Corver, J., Nieva, J.L., Bron, R., Moesby, L., Reddy, K.C., and Bittman, R. (1995). Fusion of Semliki Forest virus with cholesterol-containing liposomes at low pH: a specific requirement for sphingolipids. Mol. Membr. Biol. *12*, 143–149.

Yeager, M., Unger, V.M., and Mitra, A.K. (1999). Three-dimensional structure of membrane proteins determined by two-dimensional crystallization, electron cryomicroscopy, and image analysis. Methods Enzymol. *294*, 135–180.

Zhang, W., Mukhopadhyay, S., Pletnev, S.V., Baker, T.S., Kuhn, R.J., and Rossmann, M.G. (2002). Placement of the structural proteins in sindbis virus. J. Virol. *76*, 11645–11658.